How to cite: *Angew. Chem. Int. Ed.* **2024**, *63*, e202413323
doi.org/10.1002/anie.202413323

Supramolecular Chemistry **Hot Paper**

Ring-Size Control and Guest-Induced Circularly Polarized Luminescence in Heteroleptic $Pd_3A_3B_3$ and $Pd_4A_4B_4$ Assemblies

*Kristina E. Ebbert[+], Elie Benchimol[+], André Platzek, Christoph Drechsler, Joseph Openy, Shota Hasegawa, Julian J. Holstein, and Guido H. Clever**

Abstract: Two new structural motifs within the class of heteroleptic $Pd_nA_nB_n$ assemblies, namely *syn-cis*-$Pd_3A_3B_3$ bowls and bowl- (*syn*) or saddle- (*anti*) shaped *cis*-$Pd_4A_4B_4$ rings are introduced. All of the ten examples share a common longer fluorenone-based bis-monodentate ligand, equipped with *meta*-pyridine donor groups. The ring size (3- vs. 4-membered) and conformational preference (bowl vs. saddle) are controlled by the choice of the shorter ligand. These carry *para*-pyridine donors, different aromatic backbones (benzene, thiophene or selenophene) and either no or small or bulky endohedral substituents, serving to control the nuclearity of the heteroleptic rings through different effects (ligand angle, charge distribution or backbone bulk). Moreover, the luminescence of the fluorenone ligand is conserved in the formed architectures. Emission intensity as well as host–guest properties vary depending on the inward-pointing functions. All $Pd_3A_3B_3$ assemblies are shown to bind chiral guest BINOL bis-sulfonate which imparts its chirality to the entire host–guest complex. This results in a guest-induced circular dichroism (CD) and circularly polarized luminescence (CPL) with dissymmetry factor g_{lum} up to 10^{-3}.

Introduction

Metal-organic self-assemblies have garnered significant attention over the last decades, owing to their unique features as supramolecular receptors, catalysts and transporters.[1–3] In many cases, such assemblies can be meticulously designed by choosing proper metal nodes and organic bridging ligands and the field has produced a large variety of architectures of different sizes and shapes.[4] Recently, the design of functional assemblies[5,6] has moved into focus to realize applications in controlled guest uptake and release,[7–12] catalysis,[2,13] sensing[14] or chemical separation,[15] to name a few. With the aim of enhancing both the structural complexity and functional variety of such compounds, we, and others, have developed strategies to synthesize heteroleptic (=more than one kind of bridging ligand) assemblies, many of them serving as nanoscopic hosts.[4,6,16] Within the robust and versatile family of Pd(II)-mediated structures with bis-monodentate pyridyl bridges, most examples of multi-ligand structures reported to date are of the smallest possible nuclearity, that is Pd_2L_4,[17–24] while heteroleptic examples of higher Pd-count remain scarce. The main reason is that the assembly of larger multicomponent structures requires an even more careful consideration of the delicate balance between entropic and enthalpic factors discerning between integral self-sorting, to give a single defined heteroleptic product, and the formation of undesired statistical distributions. The groups of Fujita, Chand, Mukherjee, Severin and us have shown that heteroleptic Pd_nL_{2n} architectures of higher nuclearity ($n>3$) can be achieved by screening combinations of specific sets of organic ligands.[25–30] However, to date, the formation of heteroleptic Pd_nL_{2n} assemblies with $n=3$ has not been reported at all (and for $n=4$, only the $Pd_nA_nB_n$ pseudo-tetrahedral motif has been realized[28,29]). Only three trinuclear heteroleptic Pd(II) assemblies have been documented using ligands with denticities different than two, none of them obeying a Pd_nL_{2n} stoichiometry.[31–33] Furthermore, despite their complex structures, the examination of assemblies with $n>3$ is still in its infancy in terms of functionality and applicability.

Recently, we became particularly interested in the incorporation of chromophores into ligand backbones in order to exploit their optical properties in combination with the supramolecular characteristics of the cages they assemble.[34–36] A major aim is the realization of luminescent assemblies, applicable for sensing tasks and as chiroptical materials. However, Pd(II)-based coordination compounds showing conservation of ligand luminescence are rather rare,[28,35,37–41] as non-radiative quenching pathways are often dominated by the open-shell transition metal cation. We could recently show that architectures carrying fluorenone moieties remain luminescent even after Pd(II) coordination.[28,42,43] In addition, combining chirality and emission in modular self-assemblies has turned out to be an

[*] Dr. K. E. Ebbert,[+] E. Benchimol,[+] Dr. A. Platzek, C. Drechsler, Dr. J. Openy, Dr. S. Hasegawa, Dr. J. J. Holstein, Prof. Dr. G. H. Clever
Department of Chemistry and Chemical Biology, TU Dortmund University, Otto-Hahn-Strasse 6, 44227 Dortmund (Germany)
E-mail: guido.clever@tu-dortmund.de

[+] These authors have contributed equally

attractive strategy for the development of compounds showing Circularly Polarized Luminescence (CPL).[44] While we have recently demonstrated CPL via intra-assembly ligand-to-ligand chirality transfer,[42,43] Liu and co-workers have shown host-to-guest transfer using a chiral host and a luminescent BODIPY guest.[45] Sun and co-workers presented an emissive cage with remarkably strong CPL based on a guest-driven formation of homochiral lanthanide coordination sites.[46] In the same vein, Nitschke and co-workers showed the stereo-controlled assembly of a Cu(I) architecture displaying a reasonable dissymmetry factor.[47] In these assemblies, however, the stereochemical information is imprinted into the host molecule in the form of configurationally rather stable (=not quickly epimerizing) chiral metal centers. The chiral guest therefore steers chiral sorting at the metals that proceeds via de/recomplexation processes.

Herein, we present the first non-statistical assembly of heteroleptic *syn-cis*-$Pd_3A_3B_3$ bowls (*syn* refers to all longer ligands residing on one face of the Pd_3 plane; *cis* refers to the ligand relationship around the square-planar Pd(II) centers; from here on simply termed '$Pd_3A_3B_3$') and bowl- (*syn*) or saddle- (*anti*=alternating up-down arrangement of longer ligands) shaped *cis*-$Pd_4A_4B_4$ rings. All Pd(II) assemblies reported herein retain a certain degree of luminescence associated with the fluorenone ligand component. Moreover, the $Pd_3A_3B_3$ assemblies show an induced CPL effect when binding a chiral guest via a dynamic, non-covalent influence on the overall host conformation (Figure 1).

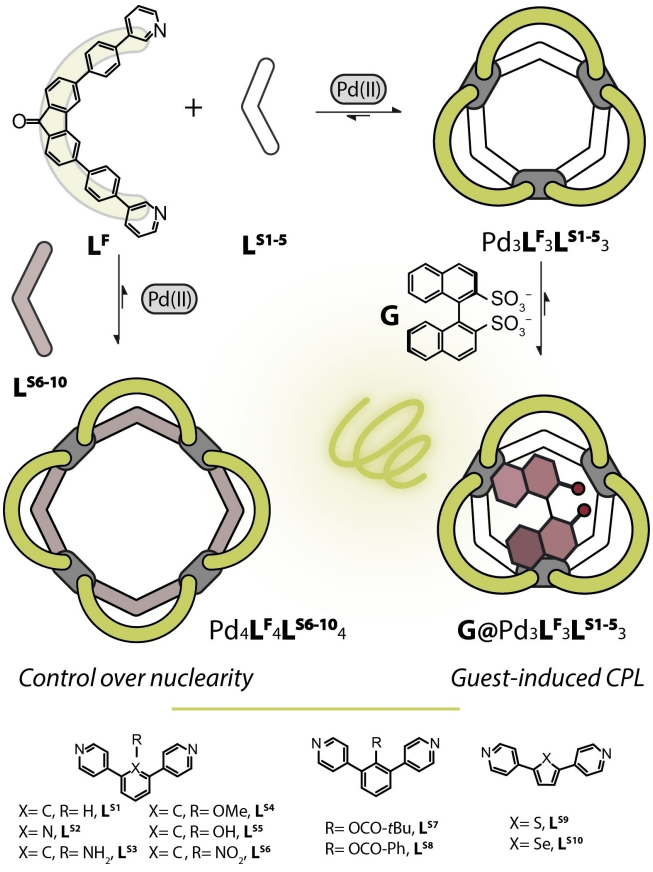

Figure 1. Formation of a *syn*-$Pd_3A_3B_3$ ring motif by self-assembly of fluorenone ligand L^F with small ligands L^{S1-5}. The obtained host structure is capable of encapsulating a chiral guest, giving rise to circularly polarized luminescence. On the other hand, shorts ligand L^{S6-10} drive the formation of bowl- and saddle-shaped $Pd_4A_4B_4$ rings.

Results and Discussion

Ligand L^F was synthesized following our previously reported procedure in a one-step Suzuki cross-coupling reaction.[42] Ligands L^{S1-10} are based on motifs reported by Fujita[48] and were obtained in similar ways from their respective dibromo precursors or by modification of the hydroxy ligand L^{S5} (Supporting Information). This synthetically simple modification of the short ligands offers the possibility of implementing various functionalities.[49–51] When combined with $[Pd(MeCN)_4](OTf)_2$ in DMSO-d_6, ligand L^F alone affords a mixture of $Pd_nL^F_{2n}$ homoleptic assemblies with the $Pd_2L^F_4$ cage being the major product. On the other hand, most of the short ligands used herein have been shown to form large hollow spheres of higher nuclearity (such as $n=12$, 24 or 48),[52] and we obtained ^{1}H NMR spectral results in accordance with these reports. The use of such ligands with obtuse angles and *para*-pyridine donors was previously shown to be a promising design principle for the formation of heteroleptic assemblies of higher nuclearity, however not including the herein introduced 3- and 4-membered ring motifs.[25,29,30]

When L^F and L^{S1} were combined in a 1:1:1 ratio with Pd(II), we observed the clean formation of a new species as attested by significant shifts of all the proton signals in the resulting ^{1}H NMR spectrum (Figure 2a–b). Further, DOSY NMR analysis showed that all the signals belong to a single assembly. The hydrodynamic radius of the assembly was calculated to be $r=14.8$ Å, already showing us that we had formed a bigger architecture than the previously described lantern-shaped $Pd_2A_2B_2$ heteroleptic cages.[53] This assumption was confirmed by ESI-MS analysis (Figure 2c). While standard ESI conditions lead to decomposition of the self-assemblies, Cryo-Spray-Ionization (CSI) ESI MS revealed the assembly's formula. The spectrum shows the species $[Pd_3L^F_3L^{S1}_3+nCF_3SO_3]^{(6-n)+}$ ($n=0$–3) with a prominent peak belonging to the 4+ species. A comparison of measured and simulated isotopic patterns of $[Pd_3L^F_3L^{S1}_3+2CF_3SO_3]^{4+}$ further supports the formation of a coordination species with a nuclearity of three and a 1:1:1 ratio between all components (Figure 2c). Other derivatives of L^{S1}, namely L^{S2-S5} (for chemical structures see Figure 1), were found to lead to the same type of structure, showing the versatility of the approach and the possibility of bringing a variety of functional groups into these assemblies (Supporting Information).

We successfully obtained crystals of $Pd_3L^F_3L^{S1}_3$ and $Pd_3L^F_3L^{S2}_3$ suitable for synchrotron diffraction experiments. The two structures unambiguously confirm the formation of the bowl-shaped rings and the 1:1:1 stoichiometry (Figure 2d–e). Interestingly, the X-ray structures of both assemblies contain two individual bowls with different

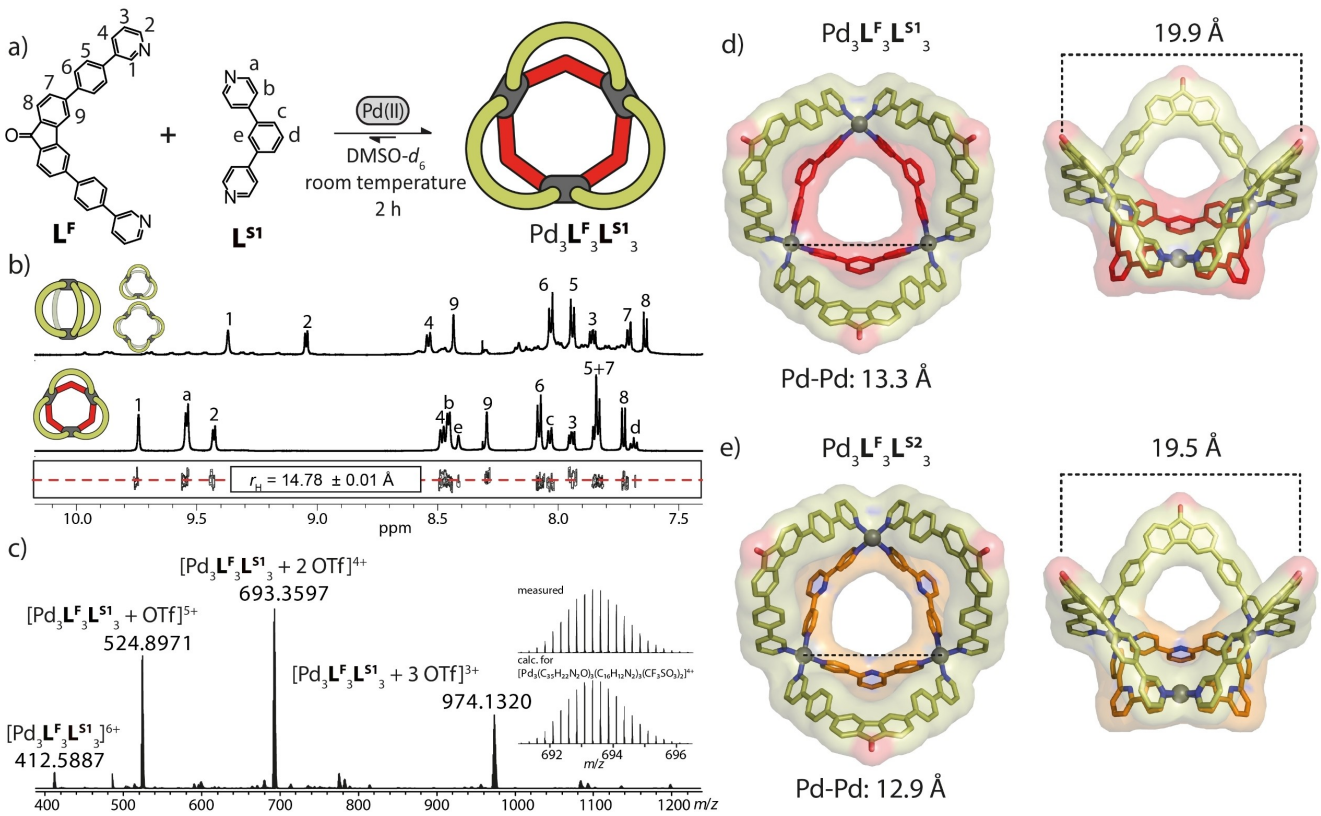

Figure 2. a) Self-assembly between $\mathbf{L^F}$ and $\mathbf{L^{S1}}$ affords a $Pd_3\mathbf{L^F}_3\mathbf{L^{S1}}_3$ ring. b) ^{1}H NMR stack (DMSO-d_6, 500 MHz) of the homoleptic assembly obtained from $\mathbf{L^F}$ (top) and $Pd_3\mathbf{L^F}_3\mathbf{L^{S1}}_3$ (bottom) with the associated DOSY trace showing the exclusive formation of a single species. c) Cryo-Spray-Ionization-MS spectra of $Pd_3\mathbf{L^F}_3\mathbf{L^{S1}}_3$ with inset showing the isotopic pattern for $[Pd_3\mathbf{L^F}_3\mathbf{L^{S1}}_3(OTf)_2]^{4+}$. X-ray crystal structures of d) $Pd_3\mathbf{L^F}_3\mathbf{L^{S1}}_3$ and e) $Pd_3\mathbf{L^F}_3\mathbf{L^{S2}}_3$ in top and side views. Both data sets contain two rings in different conformations, here only the *open* form is displayed. Pd(II)-Pd(II) and carbonyl-carbonyl distances are highlighted.

conformation ('open' and 'closed'), however, both with ligands adopting a *syn* geometry (as defined above) and both highly symmetrical (C_{3v}), likely caused by packing effects (Supporting Information). In the more open form (Figure 2d–e), $Pd_3\mathbf{L^F}_3\mathbf{L^{S1}}_3$ adopts a bowl-shaped conformation with Pd–Pd distances found to be 13.3 Å. The carbonyl-carbonyl distances are substantially bigger in the open form (19.9 Å) than in the more closed one (13.8 Å; with Pd–Pd distance = 13.4 Å), creating a defined inner void within the structure. In both cases, the pyridyl donor arms of $\mathbf{L^F}$ are rotated with respect to the planar aromatic fluorenone core in order to match the coordination vectors of the shorter ligands. The two forms, found coexisting in the solid state, highlight the conformational freedom within the assembly, despite the use of rather rigid building blocks. In a similar manner, $Pd_3\mathbf{L^F}_3\mathbf{L^{S2}}_3$ (Figure 2e) presents a Pd–Pd distance of 12.9 Å and a carbonyl-carbonyl separation of 19.5 Å (open form) vs. 12.9 Å and 13.7 Å (closed form). It is also visible that the backbone substituents right between the arms' connection atoms in the short ligands are pointing inward to the cavity of the assembly, strengthening the idea of creating endo-functionalized rings with further applicability by derivatizing these positions.

As the Pd(II)-mediated assemblies conserve their luminescence, we characterized their photophysical properties (Figure 3). The UV/Vis absorption spectrum of $Pd_3\mathbf{L^F}_3\mathbf{L^{S1}}_3$ (Figure 3a) shows an absorption maximum at 284 nm arising from the absorbance of both $\mathbf{L^F}$ and $\mathbf{L^{S1}}$ and several shoulders between 325 nm and 450 nm, characteristic of the fluorenone chromophore. The same shoulders can be found for the homoleptic assemblies of $\mathbf{L^F}$. As the spectrum of $Pd_3\mathbf{L^F}_3\mathbf{L^{S1}}_3$ resembles the sum of the spectra of the free ligands, we added a slight excess of Pd(II) cations to verify the integrity of the self-assembled heteroleptic structure at the concentration used for the optical spectroscopy experiment. As no shifts or intensity changes were observed, we conclude that the assembly is stable under the chosen conditions (further confirmed by NMR at the same dilution). Upon irradiation of $Pd_3\mathbf{L^F}_3\mathbf{L^{S1}}_3$ at $\lambda = 420$ nm, the emission of the species can be detected with a maximum at $\lambda = 520$ nm (Figure 3b). While the quantum yield of free ligand $\mathbf{L^F}$ is 13.4 % (in acetonitrile), it drops in the heteroleptic assembly to 1.1 % (Supporting Information). It is, however, slightly higher than in the homoleptic assemblies of $\mathbf{L^F}$ (0.8 %). We had observed the same partial quenching effect in lantern-shaped coordination cages with fluorenone moieties in the past.[28,42,43] The luminescence arises from π*-π transitions localized on the fluorenone ligand within the assemblies and all examined ring derivatives show emission bands with identical shapes and maxima

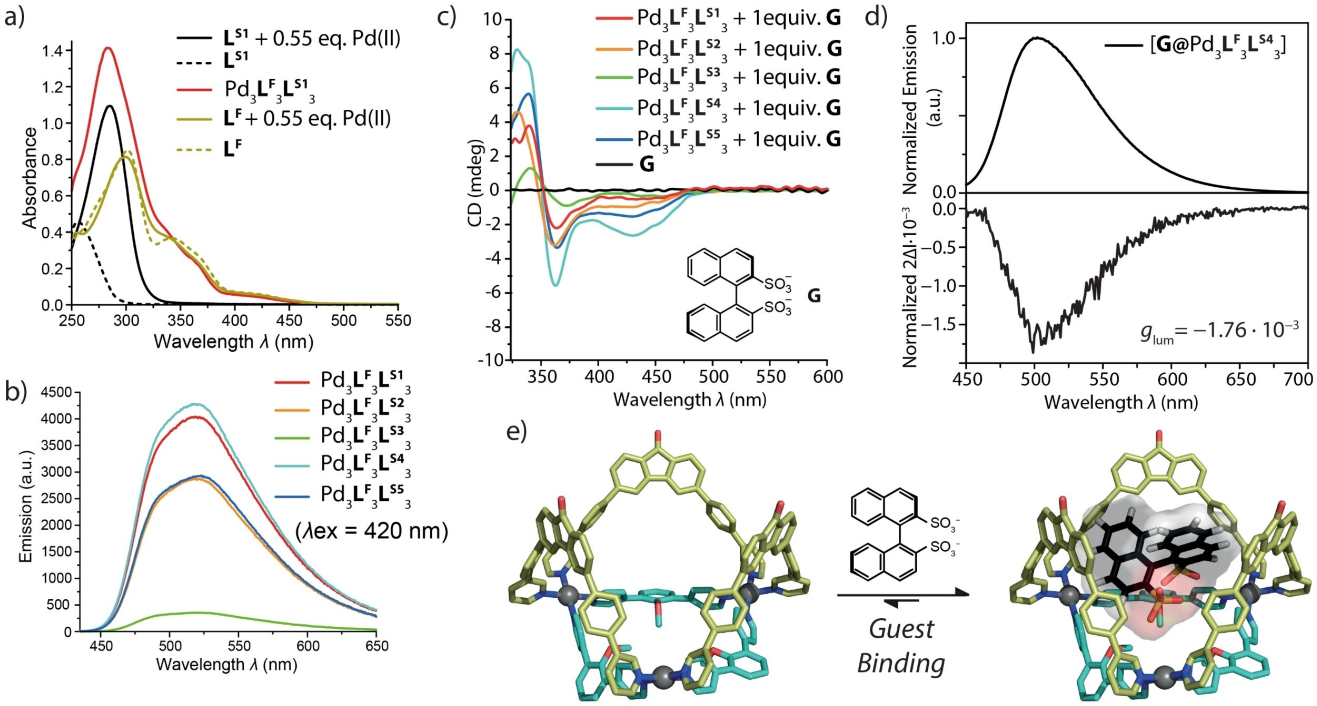

Figure 3. a) UV/Vis absorption spectra of $Pd_3L^F_3L^{S1}_3$, respective homoleptic assemblies and ligands. b) Emission spectra of the different rings (λ_{ex} = 420 nm), showing the dependence of the emission intensity on the type of the short ligand. c) CD spectra of the different rings with 1 equivalent of guest **G** added, showing chiral induction on the fluorenone moiety. d) CPL spectrum of $Pd_3L^F_3L^{S4}_3$ showing a dissymmetry factor g_{lum} of $-1.76 \cdot 10^{-3}$ at the emission maximum of the fluorenone ligand. e) DFT models (ωB97X-D/def2-SVP) of both $Pd_3L^F_3L^{S4}_3$ and $G@Pd_3L^F_3L^{S4}_3$ show the fitting of the guest in the bowl-like species (*closed* form).

(Figure 3b), however, the relative intensities were found to vary depending on the different groups installed on the short ligands. The ring $Pd_3L^F_3L^{S1}_3$, carrying a methoxy group, was found to exhibit the strongest luminescence among all (fluorescence quantum yield $\Phi_F = 1.12\,\%$).

Eventually, we studied the ability of the $Pd_3L^F_3L^{S1-5}_3$ rings to encapsulate guest molecules, considering that the bowl-shape creates a conical cavity between the three fluorenone ligands. We investigated the binding of chiral guest BINSO (**G**) with the hope of observing a guest-to-host chirality transfer (Figure 3c–e). ^{1}H NMR titration of up to 2 equivalents of the guest into a solution of $Pd_3L^F_3L^{S1}_3$ showed a shift as well as a significant broadening of all proton signals. While this demonstrates host–guest interaction, it prevented us from determining a binding constant. CSI-ESI-MS analysis further indicated host–guest formation with a 1:1 stoichiometry, as a prominent peak corresponding to $[G@Pd_3L^F_3L^{S1}_3 + OTf]^{3+}$ could be observed in the spectrum (Supporting Information). A similar behavior was observed for the other rings, both in solution and in the gas phase (Supporting Information). Notably, $Pd_3L^F_3L^{S4}_3$ shows clearer NMR titration data, with **G** having fast exchange kinetics with the host $Pd_3L^F_3L^{S4}_3$. Thus, we were able to access the binding constant for a 1:1 binding model with $K = 139 \pm 7\ M^{-1}$.

In order to check whether the chirality of the guest is transferred onto the host, we carried out circular dichroism (CD) spectroscopy experiments. Indeed, all rings clearly show a chiral induction from the bound guest with a positive band arising in the UV region and two negative ones at 360 nm and 430 nm. The latter one is characteristic of the fluorenone chromophore as we had previously observed in cages showing ligand-to-ligand chirality transfer.[42,43]

As the assemblies keep their luminescence, we were curious about their circularly polarized luminescence (CPL) properties. While $Pd_3L^F_3L^{S3}_3$ showed fast decomposition upon prolonged irradiation in the spectrometer and was thus not further investigated, all the other species show the anticipated effect. Both $Pd_3L^F_3L^{S1}_3$ and $Pd_3L^F_3L^{S2}_3$ give low dissymmetry factors g_{lum} of $-6.64 \cdot 10^{-4}$ and $-6.08 \cdot 10^{-4}$, respectively. Despite a slight improvement for $Pd_3L^F_3L^{S5}_3$ with a g_{lum} of $-9.64 \cdot 10^{-4}$, only $Pd_3L^F_3L^{S4}_3$ led to a more satisfying value of $-1.76 \cdot 10^{-3}$. This order of magnitude is in line with what we have reported for ligand-to-ligand chiral induction[42,43] as well as what has been shown by Liu in their host-to-guest chiral induction process.[45] We therefore demonstrate here the first example of a CPL-active guest-to-host chiral induction in heteroleptic assemblies. We prepared a DFT model (ωB97X-D/def2-SVP) of the guest within the cavity of the $Pd_3L^F_3L^{S4}_3$ bowl-shaped assembly, indicating that the negatively charged sulfonates point towards at least one of the three Pd(II) centers. The triangular shapes created by the three Pd(II) centers as well as the carbonyls of the fluorenones are severely distorted in the gas phase optimized structure of the host–guest complex (13.6 Å, 10.9 Å and 14.5 Å for the edges of the carbonyl

triangle). These three ligands thus fold back towards the center of the ring to form a more enclosed cavity accommodating the guest (resembling the *closed* form observed in the X-ray structures of $Pd_3\mathbf{L}^{\mathbf{F}}{}_3\mathbf{L}^{\mathbf{S1–S2}}{}_3$). This results in a stronger rotation of the pyridine donor groups of $\mathbf{L}^{\mathbf{F}}$, further deforming the luminophore-carrying part of the assembly. These distortions are the consequences of an induced-fit process between host and guest and are likely to be responsible for the emergence of a chiral answer.

We also explored two other chiral guests, namely *S*-BINPHOS and *R*-camphor sulfonate ($\mathbf{G}^{\mathbf{2}}$ and $\mathbf{G}^{\mathbf{3}}$), both being mono-anionic (Supporting Information). Both guests were found to interact with the three-membered rings, as the ^{1}H NMR spectra showed clear shifts of the inward-pointing protons. ESI-MS also confirmed association as peaks assignable to host–guest species could be observed (Supporting Information). However, when we proceeded to the CD (and CPL) experiments to probe the guest-to-host chiral induction, we observed no chiral answer for $\mathbf{G}^{\mathbf{2}}$ and only a very weak one for $\mathbf{G}^{\mathbf{3}}$ (Supporting Information). We thus conclude that no significant chiral induction occurred with these two mono-anionic guests, while bis-sulfonate BINSO (**G**) features a higher affinity and exerts a stronger structural influence on the host, both in terms of its higher charge and better fitting size.

As we were curious to see if further modification of the host was possible, we synthesized ligands $\mathbf{L}^{\mathbf{S6}}$ (carrying a nitro group), $\mathbf{L}^{\mathbf{S7–8}}$ (esters derived from phenol $\mathbf{L}^{\mathbf{S5}}$), and thiophene and selenophene-based ligands $\mathbf{L}^{\mathbf{S9–10}}$, which were already reported in the literature (Figure 4).[29] Out of these five new ligands $\mathbf{L}^{\mathbf{S6}}$, and $\mathbf{L}^{\mathbf{S8–10}}$ gave clean ^{1}H NMR spectra when mixed with $\mathbf{L}^{\mathbf{F1}}$ and Pd(II) in a 1:1:1 ratio (Figure 5a). On the other hand, $\mathbf{L}^{\mathbf{S7}}$ shows a broadening of the overall spectra, letting us infer that it forms a mixture of rings of different nuclearities. This was further confirmed by ESI-MS analysis, showing a mixture of heteroleptic assemblies $[Pd_3\mathbf{L}^{\mathbf{F}}{}_3\mathbf{L}^{\mathbf{S7}}{}_3 + xCF_3SO_3]^{(6-x)+}$ ($x = 1$–2) and $[Pd_4\mathbf{L}^{\mathbf{F}}{}_4\mathbf{L}^{\mathbf{S7}}{}_4 + xCF_3SO_3]^{(8-x)+}$ ($x = 1$–5; Supporting Information). Seemingly, bulky substituents on the inward-pointing position drive the formation of assemblies with a larger ring size. To visualize this, we modelled the three- and four-membered rings based on $\mathbf{L}^{\mathbf{S7}}$ at the semi-empirical level (PM6; Supporting Information). Indeed, in the trinuclear species, the *tert*-butyl groups are in very close contact which likely causes steric hindrance and a certain drive for also forming the tetranuclear ring in equilibrium.

The ^{1}H-DOSY NMR spectra of the other rings obtained with $\mathbf{L}^{\mathbf{S6}}$ and $\mathbf{L}^{\mathbf{S8–10}}$ also indicate significantly larger hydrodynamic radii than what we observed with ligands $\mathbf{L}^{\mathbf{S1–5}}$ (Figure 5a). CSI-MS of these samples clearly confirmed that all of these ligands exclusively lead to four-membered rings by showing peaks assigned to the formula $[Pd_4\mathbf{L}^{\mathbf{F}}{}_4\mathbf{L}^{\mathbf{S(6;8–10)}}{}_4 + xCF_3SO_3]^{(8-x)+}$ ($x = 1$–5; Figure 5b). This seems surprising for ligand $\mathbf{L}^{\mathbf{S6}}$, carrying an only three-atom nitro substituent, as it is structurally very similar to the aforementioned series $\mathbf{L}^{\mathbf{S1–5}}$ (in particular to aniline $\mathbf{L}^{\mathbf{S3}}$; all cleanly forming three-membered rings). However, the strong charge separation within the nitro group, with negative charge density delocalized over the two oxygen atoms, most probably leads

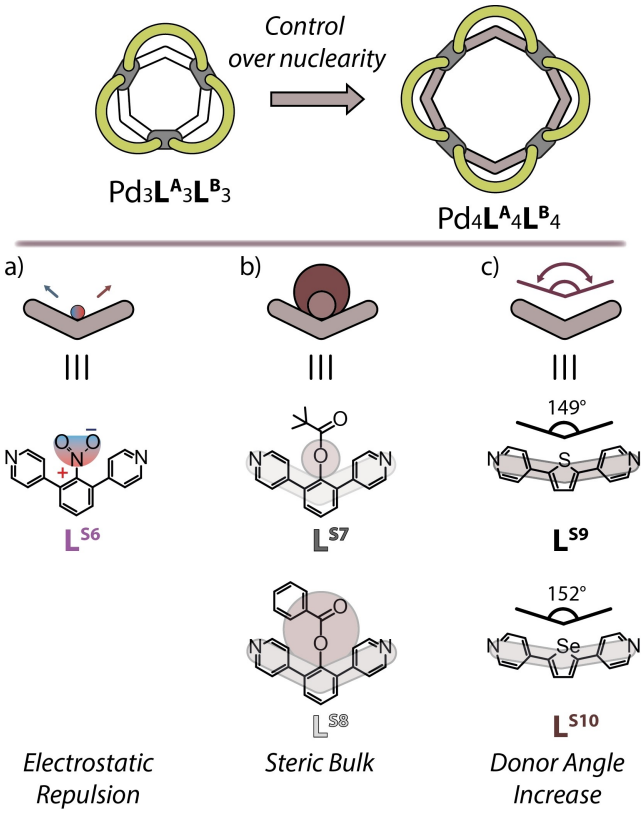

Figure 4. Three strategies to control heteroleptic ring nuclearity via a) charge repulsion, b) endohedral steric bulk and c) ligand angle.

to an enhanced electrostatic repulsion between the endohedral nitro groups of neighboring ligands in the assembly, driving the system to form the four-ring exclusively (see Supporting Information for a comparison of electrostatic potential maps of the trinuclear vs. tetranuclear species).

On the other hand, it is easier to rationalize the formation of $Pd_4A_4B_4$ structures from ligands $\mathbf{L}^{\mathbf{S8–10}}$. In the case of benzoate ester $\mathbf{L}^{\mathbf{S8}}$, the further increase in steric bulk of the endohedral substituent as compared to pivalic ester $\mathbf{L}^{\mathbf{S7}}$ now leads to the sole formation of the $Pd_4\mathbf{L}^{\mathbf{F}}{}_4\mathbf{L}^{\mathbf{S8}}{}_4$ ring (see Supporting Information). For the two remaining ligands, it was already demonstrated by Fujita for homoleptic[54] and by Severin for heteroleptic[29] assemblies that an increase in ligand binding angle results in the formation of species with higher nuclearity. This was now further verified here for $Pd_4A_4B_4$ heteroleptic rings, as the result of a better overall shape complementarity between the long and short ligands within the four-membered rings. To back this up, we carried out a series of DFT calculations (B97-3c/def2-SVP) for assemblies based on ligands $\mathbf{L}^{\mathbf{S8}}$ and $\mathbf{L}^{\mathbf{S9}}$. Therefore, we geometry-optimized and compared energies for the respective $Pd_4A_4B_4$ and $Pd_3A_3B_3$ rings and applied a correction Scheme for the different degrees of Coulomb repulsion in the 8+ and 6+ species that are dominant in the gas phase calculations (in contrast to the situation in polar solution and presence of counter anions; see Supporting Information for further details). Indeed, the in silico results are in accordance with those found

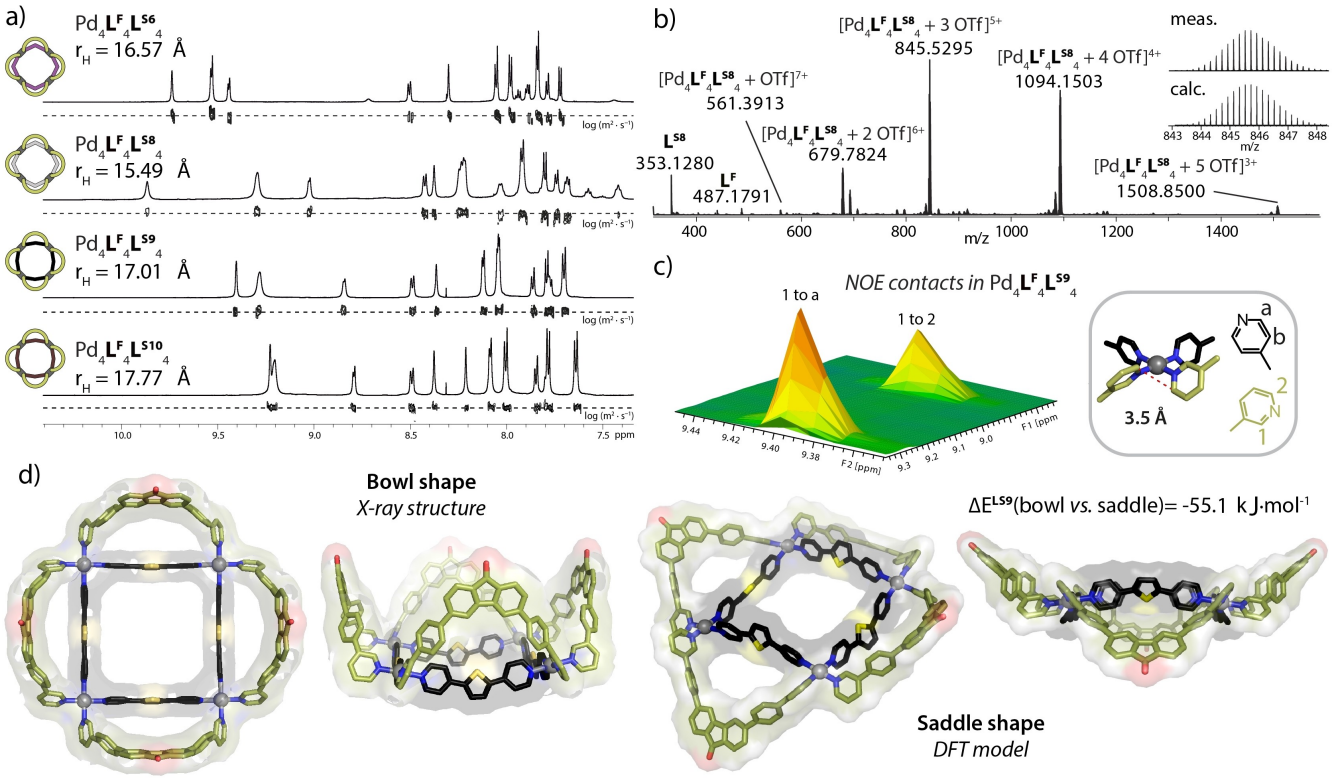

Figure 5. Four-membered heteroleptic rings. a) ^{1}H NMR and ^{1}H DOSY stack (DMSO-d_6, 500 MHz) of $Pd_4\mathbf{LF}_4\mathbf{L}^{S(6;8-10)}{}_4$ (from top to bottom). The larger hydrodynamic radius indicates bigger assemblies as compared to the three-membered rings. b) CSI-MS of $Pd_4\mathbf{L}^{F}{}_4\mathbf{L}^{S8}{}_4$ with inset showing the isotopic pattern for $[Pd_4\mathbf{L}^{F}{}_4\mathbf{L}^{S8}{}_4(OTf)_3]^{5+}$. c) 3D plot of NOE contacts in $Pd_4\mathbf{L}^{F}{}_4\mathbf{L}^{S9}{}_4$ highlighting cross-peaks indicating the saddle conformation. d) X-ray structure of $Pd_4\mathbf{L}^{F}{}_4\mathbf{L}^{S9}{}_4$ in its bowl shape conformation vs. DFT model (B97-3c/def2-SVP) of the same assembly in its saddle form.

experimentally and the higher nuclearity rings are energetically strongly favored in both cases as compared to the situation with non-bulky ligand $\mathbf{L}^{S1}$.

Interestingly, we came across another experimental observation during the NMR analysis of the heteroleptic architectures obtained from ligands $\mathbf{L}^{S8-10}$. Overlaying of their ^{1}H–^{1}H NOESY and ^{1}H–^{1}H COSY spectra reveals strong NOESY contacts between protons H1 and H2 of $\mathbf{L}^{F}$ (see Figure 5c and Supporting Information for a detailed analysis). In all of the trinuclear assemblies as well as in $Pd_4\mathbf{L}^{F}{}_4\mathbf{L}^{S6}{}_4$, this contact is rather weak because these protons are situated relatively far apart (d = 4.4–4.5 Å in $Pd_3\mathbf{L}^{F}{}_3\mathbf{L}^{S1}{}_3$; extracted from its X-ray structure). For the rings obtained from $\mathbf{L}^{S8-10}$ we therefore infer the formation of saddle-like assemblies where ligand $\mathbf{L}^{F}$ alternates between *up* and *down* positions with respect to the Pd_4-plane of the ring (for a model see Figure 5d, right). Noteworthy, this is still in accordance with the observation of one set of proton signals in the ^{1}H NMR spectra.

Eventually, we obtained single crystals from a sample of $Pd_4\mathbf{L}^{F}{}_4\mathbf{L}^{S9}{}_4$, suitable for synchrotron X-ray diffraction. The structure crystallizes in the *I4 mm* space group with one Pd(II) center and half of each ligand in the asymmetric unit (Figure 5d, left). This structure, however, shows the bowl-shaped conformer in the solid state, where all four ligands $\mathbf{L}^{F}$ are *up* with respect to the Pd_4-plane. The four Pd(II) centers form a perfect square with edges of 14.6 Å length, and the same is valid for the four carbonyl groups with a distance of 18.4 Å. We assume that this bowl conformation is a product of packing effects in the solid state, while in solution, the system may favour the saddle-type structure, resulting in a lower overall dipole moment.

We prepared DFT models (B97-3c/def2-SVP) for both the bowl and saddle conformations of the 4-ring assemblies formed from $\mathbf{L}^{S8}$ and $\mathbf{L}^{S9}$ (Supporting Information). The Coulomb-corrected gas-phase calculations clearly demonstrate that the saddle conformation is favored over the bowl with $\triangle E^{LS8}(\text{bowl}\rightarrow\text{saddle}) = -29.1\ \text{kJ}\cdot\text{mol}^{-1}$ and $\triangle E^{LS9}(\text{bowl}\rightarrow\text{saddle}) = -55.1\ \text{kJ}\cdot\text{mol}^{-1}$. These larger rings did not show any notable guest binding capabilities, probably because the saddle shape does not offer a proper inner cavity. We also did not observe any templating effect by the studied guests leading to the transformation into $Pd_3A_3B_3$ assemblies. However, the luminescence of $\mathbf{L}^{F}$ was again maintained in the four-membered rings and we characterized their photophysical properties (Supporting Information).

Conclusion

We demonstrated the first non-statistical formation of *syn-cis*-$Pd_3A_3B_3$ as well as *syn/anti-cis*-$Pd_4A_4B_4$ heteroleptic ring-like architectures by a combination of shape-complementary

assembly and backbone substituent effects, thus complementing the familiy of $Pd_nA_nB_n$ rings by motifs with $n=3$ and 4. All ten rings carry a fluorenone ligand $\mathbf{L^F}$, maintaining its luminescence after coordination to Pd(II). The $Pd_3A_3B_3$ rings are capable of binding a chiral guest which imparts its chirality to the overall assembly in a non-covalent fashion, giving rise to induced CD and CPL signals. This completes the chirality transfer Schemes in Pd(II)-based coordination cages after the ligand-to-ligand and host-to-guest phenomena had been reported previously.[42,43,45,46] We show that these two new structural motifs can be obtained from a wide variety of short ligands $\mathbf{L^{S1–5}}$ with diverse functional groups. Introduction of endohedral electrostatic repulsion (nitro ligand $\mathbf{L^{S6}}$), steric bulk (esters $\mathbf{L^{S7–8}}$), as well as angle modification ($\mathbf{L^{S9–10}}$) allows to access heteroleptic rings of a higher nuclearity. This study furthers the understanding of integrative self-sorting approaches and paves the way for the subsequent derivatization and application of non-statistical multi-component self-assemblies as selective receptors, nano-confined reaction vessels and chiroptical materials.

Supporting Information

The authors have cited additional references within the Supporting Information.[55–69]

Acknowledgments

This work was supported by the Deutsche Forschungsgemeinschaft (DFG) through GRK2376 ("Confinement-Controlled Chemistry", project number 331085229). Funded by the Deutsche Forschungsgemeinschaft (DFG, German Research Foundation) under Germany's Excellence Strategy EXC2033, project number 390677874 ("RESOLV"). We thank Laura Schneider for CSI-MS measurements. Diffraction data of $Pd_3\mathbf{L^F}_3\mathbf{L^{S1}}_3$, $Pd_3\mathbf{L^F}_3\mathbf{L^{S2}}_3$ and $Pd_4\mathbf{L^F}_4\mathbf{L^{S9}}_4$ was collected at PETRA III and processed on the Maxwell computational resources operated at DESY (Hamburg, Germany) a member of the Helmholtz Association (HGF).[70] We thank Guillaume Pompidor for assistance at synchrotron beamline P11 (I-20220526, I-20221120) and DESY user office for travel funds. Open Access funding enabled and organized by Projekt DEAL.

Conflict of Interest

The authors declare no conflict of interest.

Data Availability Statement

The data that support the findings of this study are available from the corresponding author upon reasonable request.

Keywords: self-assembly · cages · chirality · CPL · host–guest chemistry

[1] Q.-H. Ling, Z.-C. Lou, L. Zhang, T. Jin, W.-T. Dou, H.-B. Yang, L. Xu, *Chem. Soc. Rev.* **2024**, *53*, 6042–6067.
[2] Y. Fang, J. A. Powell, E. Li, Q. Wang, Z. Perry, A. Kirchon, X. Yang, Z. Xiao, C. Zhu, L. Zhang, F. Huang, H.-C. Zhou, *Chem. Soc. Rev.* **2019**, *48*, 4707–4730.
[3] T. K. Piskorz, V. Martí-Centelles, R. L. Spicer, F. Duarte, P. J. Lusby, *Chem. Sci.* **2023**, *14*, 11300–11331.
[4] C. T. McTernan, J. A. Davies, J. R. Nitschke, *Chem. Rev.* **2022**, *122*, 10393–10437.
[5] J. E. M. Lewis, *Chem. Commun.* **2022**, *58*, 13873–13886.
[6] S. Pullen, J. Tessarolo, G. H. Clever, *Chem. Sci.* **2021**, *12*, 7269–7293.
[7] D. Zhang, T. K. Ronson, S. Güryel, J. D. Thoburn, D. J. Wales, J. R. Nitschke, *J. Am. Chem. Soc.* **2019**, *141*, 14534–14538.
[8] V. Croué, S. Goeb, G. Szalóki, M. Allain, M. Sallé, *Angew. Chem. Int. Ed.* **2015**, *55*, 1746–1750.
[9] W. Cullen, S. Turega, C. A. Hunter, M. D. Ward, *Chem. Sci.* **2014**, *6*, 625–631.
[10] A. Ghosh, L. Slappendel, B.-N. T. Nguyen, L. K. S. von Krbek, T. K. Ronson, A. M. Castilla, J. R. Nitschke, *J. Am. Chem. Soc.* **2023**, *145*, 3828–3832.
[11] H. Lee, J. Tessarolo, D. Langbehn, A. Baksi, R. Herges, G. H. Clever, *J. Am. Chem. Soc.* **2022**, *7*, 3099–3105.
[12] T. Y. Kim, R. A. S. Vasdev, D. Preston, J. D. Crowley, *Chem. Eur. J.* **2018**, *24*, 14878–14890.
[13] C. Tan, D. Chu, X. Tang, Y. Liu, W. Xuan, Y. Cui, *Chem. Eur. J.* **2019**, *25*, 662–672.
[14] A. Brzechwa-Chodzyńska, W. Drożdż, J. Harrowfield, A. R. Stefankiewicz, *Coord. Chem. Rev.* **2021**, *434*, 213820.
[15] D. Zhang, T. K. Ronson, Y.-Q. Zou, J. R. Nitschke *Nat. Chem. Rev.* **2021**, *5*, 168–182.
[16] J. E. M. Lewis, *Trends Chem.* **2023**, *5*, 717–719.
[17] Y. Liu, S. Liao, W. Dai, Q. Bai, S. Lu, H. Wang, X. Li, Z. Zhang, P. Wang, W. Lu, Q. Zhang, *Angew. Chem. Int. Ed.* **2023**, *62*, e202217215.
[18] D. Preston, J. E. Barnsley, K. C. Gordon, J. D. Crowley, *J. Am. Chem. Soc.* **2016**, *138*, 10578–85.
[19] J. E. M. Lewis, A. Tarzia, A. J. P. White, K. E. Jelfs, *Chem. Sci.* **2020**, ***11***, 677–683.
[20] J. E. M. Lewis, *Angew. Chem. Int. Ed.* **2022**, *61*, e202212392.
[21] M. Yamashina, T. Yuki, Y. Sei, M. Akita, M. Yoshizawa, *Chem. Eur. J.* **2015**, *21*, 4200–4204.
[22] A. M. Johnson, R. J. Hooley, *Inorg. Chem.* **2011**, *50*, 4671–4673.
[23] B. Chen, J. J. Holstein, A. Platzek, L. Schneider, K. Wu, G. H. Clever, *Chem. Sci.* **2022**, *13*, 1829–1834.
[24] K. Wu, E. Benchimol, A. Baksi, G. Clever, *Nat. Chem.* **2023**, *16*, 584–591.
[25] Q. Sun, S. Sato, M. Fujita, *Angew. Chem. Int. Ed.* **2014**, *53*, 13510–13513.
[26] S. Prusty, K. Yazaki, M. Yoshizawa, D. K. Chand, *Chem. Eur. J.* **2017**, *23*, 12456–12461.
[27] P. Howlader, P. Das, E. Zangrando, P. S. Mukherjee, *J. Am. Chem. Soc.* **2016**, *138*, 1668–1676.
[28] J. Tessarolo, H. Lee, E. Sakuda, K. Umakoshi, G. H. Clever, *J. Am. Chem. Soc.* **2021**, *143*, 6339–6344.
[29] R. Li, F. Fadaei-Tirani, R. Scopelliti, K. Severin, *Chem. Eur. J.* **2021**, *27*, 9439–9445.
[30] S. Sudan, R.-J. Li, S. M. Jansze, A. Platzek, R. Rudolf, G. H. Clever, F. Fadaei-Tirani, R. Scopelliti, K. Severin, *J. Am. Chem. Soc.* **2021**, *143*, 1773–1778.
[31] K. Wu, B. Zhang, C. Drechsler, J. J. Holstein, G. H. Clever, *Angew. Chem. Int. Ed.* **2020**, *60*, 6403–6407.

[32] J. A. Findlay, K. M. Patil, M. G. Gardiner, H. I. MacDermott-Opeskin, M. L. O'Mara, P. E. Kruger, D. Preston, *Chem. Asian J.* **2022**, *17*, e202200093.
[33] H. Lee, T. H. Noh, O. Jung, *Angew. Chem. Int. Ed.* **2016**, *55*, 1005–1009.
[34] I. Regeni, B. Chen, M. Frank, A. Baksi, J. J. Holstein, G. H. Clever, *Angew. Chem. Int. Ed.* **2021**, *60*, 5673–5678.
[35] I. Regeni, R. Chowdhury, K. Terlinden, S. Horiuchi, J. J. Holstein, S. Feldmann, G. H. Clever, *Angew. Chem. Int. Ed.* **2023**, *62*, e202308288.
[36] A. Walther, I. Regeni, J. J. Holstein, G. H. Clever, *J. Am. Chem. Soc.* **2023**, *145*, 25365–25371.
[37] A. Schmidt, M. Hollering, J. Han, A. Casini, F. E. Kühn, *Dalton Trans.* **2016**, *45*, 12297–12300.
[38] A. B. S. Elliott, J. E. M. Lewis, H. van der Salm, C. J. McAdam, J. D. Crowley, K. C. Gordon, *Inorg. Chem.* **2016**, *55*, 3440–3447.
[39] D. Dalmau, E. P. Urriolabeitia, *Molecules* **2023**, *28*, 2663.
[40] D. R. Martir, D. B. Cordes, A. M. Z. Slawin, D. Escudero, D. Jacquemin, S. L. Warriner, E. Zysman-Colman, *Chem. Commun.* **2018**, *54*, 6016–6019.
[41] D. R. Martir, D. R. Martir, D. Escudero, D. Jacquemin, D. B. Cordes, A. M. Z. Slawin, H. A. Fruchtl, S. L. Warriner, E. Z. Colman, *Chem. Eur. J.* **2017**, *23*, 14358–14366.
[42] K. Wu, J. Tessarolo, A. Baksi, G. H. Clever, *Angew. Chem. Int. Ed.* **2022**, *61*, e202205725.
[43] J. Tessarolo, E. Benchimol, A. Jouaiti, M. W. Hosseini, G. H. Clever, *Chem. Commun.* **2023**, *59*, 3467–3470.
[44] X. Chen, S. Zhang, X. Chen, Q. Li, *ChemPhotoChem* **2022**, *6*, e202100256.
[45] X. Tang, H. Jiang, Y. Si, N. Rampal, W. Gong, C. Cheng, X. Kang, D. Fairen-Jimenez, Y. Cui, Y. Liu, *Chem* **2021**, *7*, 2771–2786.
[46] S.-J. Hu, X.-Q. Guo, L.-P. Zhou, D.-N. Yan, P.-M. Cheng, L.-X. Cai, X.-Z. Li, Q.-F. Sun, *J. Am. Chem. Soc.* **2022**, *144*, 4244–4253.
[47] H. Zhu, L. Pesce, R. Chowdhury, W. Xue, K. Wu, T. K. Ronson, R. H. Friend, G. M. Pavan, J. R. Nitschke, *J. Am. Chem. Soc.* **2024**, *146*, 2379–2386.
[48] M. Tominaga, K. Suzuki, M. Kawano, T. Kusukawa, T. Ozeki, S. Sakamoto, K. Yamaguchi, M. Fujita, *Angew. Chem. Int. Ed.* **2004**, *43*, 5621–5625.
[49] K. Harris, D. Fujita, M. Fujita, *Chem. Commun.* **2013**, *49*, 6703–6712.
[50] Y. Ueda, H. Ito, D. Fujita, M. Fujita, *J. Am. Chem. Soc.* **2017**, *139*, 6090–6093.
[51] D. Fujita, K. Suzuki, S. Sato, M. Yagi-Utsumi, Y. Yamaguchi, N. Mizuno, T. Kumasaka, M. Takata, M. Noda, S. Uchiyama, K. Kato, M. Fujita, *Nat. Commun.* **2012**, *3*, 1093.
[52] E. O. Bobylev, D. A. Poole, B. Bruin, J. N. H. Reek, *Chem. Eur. J.* **2021**, *27*, 12667–12674.
[53] K. Wu, E. Benchimol, A. Baksi, G. H. Clever, *Nat. Chem.* **2024**, 1–8.
[54] D. Fujita, Y. Ueda, S. Sato, N. Mizuno, T. Kumasaka, M. Fujita, *Nature* **2016**, *540*, 563–566.
[55] A. Jerschow, N. Müller, *J. Magn. Reson.* **1997**, *125*, 372–375.
[56] J. E. Tanner, E. O. Stejskal, *J. Chem. Phys.* **1968**, *49*, 1768–1777.
[57] A. Macchioni, G. Ciancaleoni, C. Zuccaccia, D. Zuccaccia, *Chem. Soc. Rev.* **2007**, *37*, 479–489.
[58] D. Fujita, H. Yokoyama, Y. Ueda, S. Sato, M. Fujita, *Angew. Chem. Int. Ed.* **2015**, *54*, 155–158.
[59] L. Neukirch, M. D. Kulas, J. J. Holstein, G. H. Clever, *Chem. Eur. J.* **2024**, e202400132.
[60] A. Burkhardt, T. Pakendorf, B. Reime, J. Meyer, P. Fischer, N. Stübe, S. Panneerselvam, O. Lorbeer, K. Stachnik, M. Warmer, P. Rödig, D. Göries, A. Meents, *European. Phys. J. Plus.* **2016**, *131*, 56.
[61] W. Kabsch, *Acta Crystallogr Sect D Biological Crystallogr.* **2010**, *66*, 125–132.
[62] G. M. Sheldrick, *Acta Crystallogr. Sect. Found. Adv.* **2015**, *71*, 3–8.
[63] G. M. Sheldrick, *Acta Crystallogr. Sect. C Struct. Chem.* **2015**, *71*, 3–8.
[64] C. B. Hübschle, G. M. Sheldrick, B. Dittrich, *J. Appl. Crystallogr.* **2011**, *44*, 1281–1284.
[65] D. Kratzert, J. J. Holstein, I. Krossing, *J. Appl. Crystallogr.* **2015**, *48*, 933–938.
[66] D. Kratzert, I. Krossing, *J. Appl. Crystallogr.* **2018**, *51*, 928–934.
[67] A. Thorn, B. Dittrich, G. M. Sheldrick, *Acta Crystallogr. Sect. Found Crystallogr.* **2012**, *68*, 448–451.
[68] A. L. Spek, *Acta Crystallogr. Sect. C Struct. Chem.* **2015**, *71*, 9–18.
[69] A. L. Spek, *Acta Crystallogr. Sect. D Biological Crystallogr.* **2009**, *65*, 148–155.
[70] Deposition Number(s) 2331613 (for $Pd_3\mathbf{L}^{\mathbf{F}}{}_3\mathbf{L}^{\mathbf{S1}}{}_3$), 2331614 (for $Pd_3\mathbf{L}^{\mathbf{F}}{}_3\mathbf{L}^{\mathbf{S2}}{}_3$), 2331615 ($Pd_4\mathbf{L}^{\mathbf{F}}{}_4\mathbf{L}^{\mathbf{S9}}{}_4$) contain the supplementary crystallographic data for this paper. These data are provided free of charge by the joint Cambridge Crystallographic Data Centre and Fachinformationszentrum Karlsruhe Access Structures service.

Manuscript received: July 15, 2024
Accepted manuscript online: July 29, 2024
Version of record online: September 20, 2024